

The Three-Dimensional Structure of the Gallium Complex of Azoverdin, a Siderophore of *Azomonas macrocytogenes* ATCC 12334, Determined by NMR Using Residual Dipolar Coupling Constants[†]

Emeric Wasielewski,[‡] R. Andrew Atkinson,[‡] Mohamed A. Abdallah,[§] and Bruno Kieffer^{*‡}

Laboratoire de Biologie et de Génomique Structurales, Groupe de RMN, UMR 7104 CNRS, ESBS, bd Sébastien Brant, 67400 Illkirch, France, and Laboratoire de Chimie Microbienne, Département des Récepteurs et Protéines Membranaires, UPR 9050 CNRS, ESBS, bd Sébastien Brant, 67400 Illkirch, France

Received April 18, 2002; Revised Manuscript Received July 23, 2002

ABSTRACT: In iron-deficient conditions, *Azomonas macrocytogenes* ATCC 12334 excretes a fluorescent siderophore called azoverdin, which is composed of a six-amino-acid peptide chain linked to a chromophore. Azoverdin chelates iron(III) very strongly, solubilizing it and transporting it back into the cells using an outer-membrane receptor. This compound is related to the pyoverdins, the peptidic siderophores of *Pseudomonas*, but differs in the site on the chromophore at which the peptide is covalently linked. This feature identifies azoverdin as a member of a new class of pyoverdins: the isopyoverdins. We report the three-dimensional structure of azoverdin–Ga(III) in solution. The use of orientational constraints obtained from the measurement of residual dipolar couplings using samples dissolved in a liquid crystalline medium allowed us to define the absolute configuration of the metal complex, which is Δ . The structure is characterized by a U-shape adopted by the peptide chain, with the N^δ-acetyl-N^δ-hydroxyornithine side chains adopting extended conformations in order to chelate the gallium ion. This conformation leaves a large open space permitting access to the gallium ion. The structural consequences of the particular isopyoverdin chemical structure are discussed in the context of the three-dimensional structures of other pyoverdins.

*Azomonas macrocytogenes*¹ is a nitrogen-fixing bacterium that transforms atmospheric nitrogen into ammonia (1, 2). Only a relatively small number of microorganisms termed diazotrophs (3) are capable of carrying out this process, and all other organisms depend directly or indirectly upon them for their supply of nitrogenated compounds. This biological reduction of atmospheric nitrogen into ammonia (nitrogen fixation) is performed by a multimeric enzyme called *nitrogenase*, which catalyzes the conversion of molecular nitrogen (N₂) into two molecules of ammonia (NH₃). Nitrogenases occur in *Rhizobia*, bacteria living symbiotically in some plants roots (beans, peas, alfalfa), in free soil bacteria

such as *Azotobacter*, *Klebsiella*, *Azospirillum*, *Azomonas*, etc., and in blue algae (cyanobacteria). These enzymes possess two proteic compartments, one containing iron (Fe–protein) and the other either molybdenum and iron (Mo–Fe–protein) or vanadium and iron (V–Fe–protein). These metalloproteins are all rapidly inactivated by molecular oxygen (4).

Iron metabolism by the microorganisms generally requires the biosynthesis of low molecular weight compounds (300–2000 Da) called siderophores (5). These molecules, which are commonly excreted into the culture medium, chelate iron(III) very strongly, solubilizing it and transporting it back into the cells using an ATP-dependent high affinity transport system (6). Under iron-deficient conditions, *Azomonas macrocytogenes* ATCC 12334 excretes a fluorescent siderophore called azoverdin (7), which utilizes an outer-membrane receptor to transport iron into the cell (8). Azoverdin is a chromopeptide very closely related in structure to pyoverdins, the peptidic siderophores of the fluorescent *Pseudomonas* (9). Pyoverdins are composed of a fluorescent chromophore derived from 2,3-diamino-6,7-dihydroxyquinoline, bound via a carboxylic acid group to the N-terminus of an oligopeptide of 6–12 amino acids of varying chirality and composition with a linear (10–17), partially cyclic (18–26), or fully cyclic (27) backbone.

All these pyoverdins or pyoverdin-like siderophores possess three iron(III)-specific bidentate groups: the catechol group of the chromophore, one hydroxamate group at the end of the peptidic chain, and either an additional hydrox-

[†] E.W. was supported by a fellowship from the French “Ministère de la Recherche et de l’Enseignement Supérieur”.

^{*} Corresponding author. Tel: 33 3 90 24 47 22. Fax: 33 3 90 24 47 18. E-mail: kieffer@esbs.u-strasbg.fr.

[‡] Laboratoire de Biologie et de Génomique Structurales.

[§] Laboratoire de Chimie Microbienne.

¹ Abbreviations: common amino acids, three-letter code; AcOHOrn, N^δ-acetyl-N^δ-hydroxyornithine; Chr, chromophore; Dab, 2,4-diaminobutyric acid; DEAE, diethyl-aminoethyl; DQF COSY, double quantum filtered correlated spectroscopy; DHPC, 1,2-dihexanoyl-*sn*-glycero-3-phosphocholine; DMPC, 1,2-dimyristoyl-*sn*-glycero-3-phosphocholine; GARP, globally optimized alternating-phase rectangular pulses; HMQC, heteronuclear multiple-quantum coherence spectroscopy; Hse, homoserine; HOHAHA, homonuclear Hartmann–Hahn spectroscopy; HSQC, heteronuclear single-quantum coherence spectroscopy; NOESY, nuclear Overhauser enhancement spectroscopy; RDC, residual dipolar coupling; rmsd, root-mean-square deviation; ROESY, rotating frame Overhauser enhancement spectroscopy; TTAB, tetradecyltrimethylammonium bromide; CT-HMQC, constant-time heteronuclear multiple quantum coherence spectroscopy.

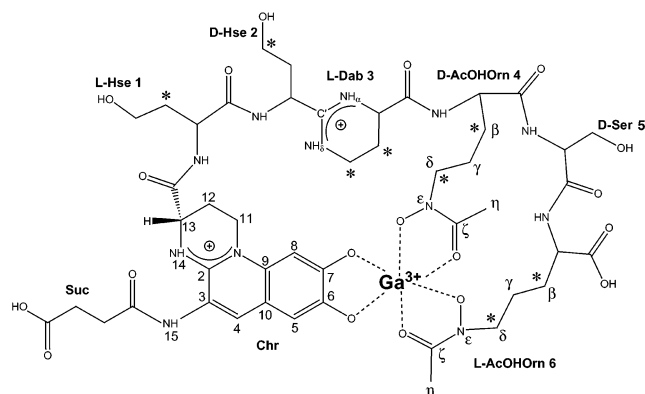


FIGURE 1: Primary structure of azoverdin. Sites at which protons could be stereospecifically assigned are indicated by asterisks.

amate group or a hydroxycarboxylic acid group in the middle of the chain. These bidentate groups bind iron(III) with extremely high affinity giving very stable octahedral complexes. The primary structure of azoverdin was first reported to be a chromopeptide with a chromophore derived from 2,3-diamino-6,7-dihydroxyquinoline bound to a peptide chain containing two homoserines, one serine and two N^{δ} -hydroxyornithines (15, 28). In addition, a new amidine type of amino acid is present in the peptide chain: (1'-amino,3'-hydroxy)-2-propyl-4-carboxy-3,4,5,6-tetrahydro-pyrimidine, resulting from the condensation of one homoserine with 2,4-diaminobutyric acid (Dab). This chemical structure is reminiscent of the pyoverdins, where a serine (*Pseudomonas fluorescens* CCM 2298 and CCM 2299), a glutamine (*P. fluorescens* ATCC 17400), a tyrosine (desferriferribactin, *P. fluorescens* ATCC 13525 and *P. chlororaphis* ATCC 9446) (24), or a hydroxyaspartic acid (*P. putida* G4R) (17) are linked with the 2,4-diaminobutyric acid.

Two primary sequences of azoverdin have been published that differed in the sequence of the peptide chain and in the site of covalent linkage on the chromophore (15, 16). The use of a triple resonance HNCA experiment on ^{15}N -labeled azoverdin-Ga(III) with ^{13}C at natural abundance (29) provided us with the connectivities required to confirm the primary sequence proposed by Milchalke (16) and allowed completion of proton, nitrogen, and carbon assignments of azoverdin-Ga(III). The gallium ion was used as a known isosteric diamagnetic substitute for iron(III). In the primary sequence of azoverdin (Figure 1), the Dab residue is located in the third position of the peptide chain which is bound to the chromophore at position C-13. This unusual linkage point led to the definition of a new class of pyoverdin named isopyoverdins (16).

We report here the three-dimensional structure of azoverdin-Ga(III) in solution. The usual set of distance constraints derived from interproton nuclear Overhauser effects (NOE) was complemented by orientational constraints obtained from the measurement of residual dipolar couplings using samples dissolved in liquid crystalline media (30, 31). Together with dihedral angle values derived from coupling constants, these data allowed us to define a unique conformation out of the 16 possible conformations of the chiral center around the gallium ion. The specific structural features of azoverdin-Ga(III), the first reported structure of an isopyoverdin, are discussed and compared to those of other pyoverdins for which three-dimensional structures are known.

EXPERIMENTAL PROCEDURES

Sample Preparation. Bacteria were grown aerobically for 48 h in iron-free Burk medium (32) containing 0.2 g L^{-1} $(^{15}\text{NH}_4)_2\text{SO}_4$ and 1% mannitol (w/v) to replace glucose (33).

Azoverdin-Ga(III) complex was prepared and characterized as described in Bernardini et al. (15). In brief, azoverdin pure free ligand (21 mg) was dissolved in 2 mL of distilled water and the mixture treated with 5 equiv of $0.1 \text{ M Ga}(\text{NO}_3)_3 \cdot 9\text{H}_2\text{O}$. The solution was kept for 1 h at room temperature and applied first on a CM-Sephadex column C25 ($20 \times 1.5 \text{ cm}$) and then on a DEAE 25 Sephadex column ($20 \times 1.5 \text{ cm}$). Both columns were eluted with 25 mM pyridine/acetic acid buffer (pH 5.0). The yield of pure complex was 9 mg, and the purity was checked by mass spectrometry.

Most NMR experiments were conducted on a sample containing 10.4 mM azoverdin-Ga(III) in $\text{H}_2\text{O}:\text{D}_2\text{O}$ 11:1 at pH 3.6 and at 298 K. For residual dipolar coupling measurements, DHPC and DMPC (Avanti Polar Lipids Inc., Alabaster, AL) were dissolved together in a small volume of buffer (10 mM phosphate, pH 6.5, 0.02% NaN_3) with a 3:1 molar ratio. TTAB was added at 2.4 mM to increase bicelle stability. The NMR sample was then prepared by mixing one volume of bicelle to two volumes of siderophore in solution.

NMR Spectroscopy. NMR experiments were performed on Bruker AMX 500 and DRX 600 spectrometers. Standard two-dimensional proton experiments (DQF-COSY (34), HOHAHA (35), NOESY (36), and off-resonance ROESY (37)) were modified to include nitrogen decoupling during t_1 and t_2 time domains. Decoupling during t_1 was achieved by inserting a 180° pulse on ^{15}N in the middle of the ^1H chemical shift evolution time, whereas decoupling during acquisition was achieved using a GARP decoupling sequence (38). The spectra were acquired in the phase-sensitive mode (39), with a spectral width of 8012.82 Hz in both dimensions and a relaxation delay of 3 s. Solvent suppression was achieved using a WATERGATE sequence (40). Mixing times were set to 60 ms for the HOHAHA spectrum, 400 and 800 ms for the NOESY spectra, and 400 ms for the off-resonance ROESY spectrum. For interproton distance measurement, a NOE buildup experiment was performed by recording a further set of eight ^{15}N -decoupled NOESY experiments with mixing times ranging from 30 to 500 ms. In these spectra, the spectral widths were set to 6024.86 Hz in both dimensions, and the relaxation delay was 2.5 s. Typically, 8 or 16 scans of 2K data points were acquired for each of the 512 t_1 increments, giving a final matrix size of $2\text{K} \times 1\text{K}$. Processing was performed using XWIN NMR (Bruker) or FELIX 2.1 (Accelrys Inc., Burlington, MA) software. Typically, 90° -shifted squared sine-bell apodization was applied prior to Fourier transform in both dimensions, except for the DQF-COSY spectrum where an unshifted sine-bell was used in both dimensions for resolution enhancement.

HN Exchange. Slowly exchanging amide protons were identified from a series of NOESY spectra with a mixing time of 200 ms recorded at 298 K after addition of D_2O to the lyophilized sample.

Coupling Constant Measurements. $^3J_{\text{HN-H}\alpha}$ coupling constants were measured from a set of 13 constant-time two-

dimensional ^1H - ^{15}N CT-HMQC-J spectra (41), with constant times ranging from 8 to 32 ms with 2 ms increments. Spectra were recorded in phase-sensitive mode, using the States-TPPI method (42), with spectral widths of 7002.8 and 5000 Hz in the F2 and F1 dimensions, respectively. The relaxation delay was set to 2.5 s, and the water resonance was suppressed using a low power presaturation pulse. The intensities of the ^{15}N -proton correlation peaks were measured using FELIX 2.1 software, and $^3J_{\text{HN-H}\alpha}$ values were extracted from a nonlinear fit of the time-dependent intensities using MATLAB software (The MathWorks Inc., Natick, MA). $^3J_{\text{N-H}\beta}$ coupling constants were measured using a NOESY experiment recorded without ^{15}N decoupling in the F1 dimension (43). The $^3J_{\text{N-H}\beta}$ values were estimated from the relative displacement of the two HN-H β cross-peaks corresponding to the α and β spin states of the nitrogen. One bond $^1J_{\text{N-H}}$ coupling constants were measured using an ^{15}N - ^1H HSQC spectrum recorded without nitrogen decoupling during acquisition. The spectrum was recorded using the sensitivity enhanced echo-antiecho scheme (44), with spectral widths of 8012 and 3000 Hz in F2 and F1 dimensions, respectively. The $^1J_{\text{N-H}}$ values were measured on the relevant F2 cross-sections of the HSQC spectrum in XWIN NMR. Residual dipolar coupling contributions were obtained by measuring $^1J_{\text{N-H}}$ and $^3J_{\text{HN-H}\alpha}$ values for the sample dissolved in the DHPC/DMPC containing buffer at 308 K (nematic phase). The isotropic phase $^1J_{\text{N-H}}$ and $^3J_{\text{HN-H}\alpha}$ values were measured on a sample dissolved in water at 305 K.

Distance Constraints. Interproton distance constraints were obtained from the initial rate of the NOE cross-peak intensity buildup curves. The measured buildup rates were translated into distances using the rate observed for the cross-peak between the aromatic protons H4 and H5 of the chromophore as a calibration distance. A tolerance of $+0.3/-0.4$ or ± 0.5 Å was assigned to the distance value according to the quality of the buildup curve. The upper bound of distances involving pseudoatoms was increased by 0.5 Å.

Structure Calculations. Most calculations were carried out on Compaq bi-processor EV6-500 MHz computers using standard protocols (sa, refine, accept) in X-PLOR 3.851 (45). The standard topology and parameter files (topallhdg.pro and parallhdg.pro) were modified to allow definition of the chromophore and the nonstandard residues of azoverdin: homoserines, N $^{\delta}$ -acetyl-N $^{\delta}$ -hydroxyornithines and 2,4-diaminobutyric acid. Nonbonded parameters for the Ga(III) ion were set to the same values used for iron atoms in standard X-PLOR parameters sets (the radii of the two ions are similar).

For calculations using residual dipolar coupling constraints, the set of starting structures was refined using XPLOR-NIH, in which pseudopotentials for dipolar coupling constraints are incorporated (46). The alignment tensor orientation is represented by a four-atom pseudomolecule, placed at 100 Å from the complex, whose bonds correspond to the three orthogonal alignment axes. The pseudo complex orientation is allowed to float freely during the structure calculation since the direction of the alignment tensor is not known a priori.

First, a simulated annealing protocol was applied performing 12 000 steps at high temperature (2000 K) and 12 000 steps during cooling to 100 K, with a time step of 1 fs for dynamics. Only constraints defining the coordination site

geometry were applied, using a soft NOE energy function. The resulting structures were then refined with 6000 steps for cooling to 100 K from an initial temperature of 2000 K. All constraints were included at this stage using a square-well NOE energy function. Structures were visualized using MOLMOL 2.6 (47).

A total of 82 constraints derived from NOE buildup curves was used to define interproton distances, applying standard pseudoatom corrections where required. Of these constraints, 36 were intraresidue, 19 sequential, and 27 longer-range. Coordination of the Ga(III) ion was defined using distance constraints between each of six oxygen atoms (Chr O6, Chr O7, AcOHOrn4 O ϵ , AcOHOrn4 O ζ , AcOHOrn6 O ϵ , AcOHOrn6 O ζ) and the metal ion. Improper angle definitions were used to fix the Ga(III) ion in chelating group planes. Coordination geometry was imposed by three improper angles between coordinating oxygen atoms (two oxygen atoms from the same chelating group and two at the opposite side of the octahedron) set to $\pm 54.8^\circ$ ($\pm 15^\circ$). Distances ($d_{\text{Ga-O}}$) were set to cover the range of values found in crystallographic studies of siderophores: 2.04 ± 0.10 Å. A force constant of $50.0 \text{ kcal.mol}^{-1}.\text{Å}^{-2}$ was applied to all distance constraints. Distances between pairs of coordinating oxygen atoms on adjacent vertexes of the octahedron were set to $d_{\text{O-O}} = 2.85 \pm 0.10$ Å.

RESULTS

Resonance Assignment. Assignments of ^1H , ^{15}N , and ^{13}C resonances of azoverdin-Ga(III) have been reported previously (29). The use of a triple resonance HNCA experiment recorded on a ^{15}N -labeled sample allowed us to establish that the primary sequence of azoverdin was indeed that published by Michalke et al. (16). The chemical structure of azoverdin (Figure 1) differs from other pyoverdin structures by the peptide anchoring point to the chromophore. In azoverdin, this anchoring point is located at position C13 of the chromophore, whereas it is located at position C11 in other pyoverdin structures. This structural difference led to the definition of a new class of pyoverdins named isopyoverdins (16).

The analysis of HN-H β and H α -H β distances, together with $^3J_{\text{H}\alpha\text{-H}\beta}$ and $^3J_{\text{N-H}\beta}$ coupling constants, allowed the stereospecific assignment of four sets of H β methylene protons. Thus, the H β protons of residues Hse1 (H β 1: 1.84 ppm; H β 2: 1.88 ppm), Dab3 (H β 1: 2.16 ppm; H β 2: 2.37 ppm), AcOHOrn4 (H β 1: 1.76 ppm; H β 2: 1.89 ppm) and AcOHOrn6 (H β 1: 1.62 ppm; H β 2: 1.84 ppm) were assigned stereospecifically. During the course of the structure calculation, it was possible to further assign stereospecifically the H γ protons of Hse2 (H γ 1: 3.64 ppm; H γ 2: 3.69 ppm) and Dab3 (H γ 1: 2.66 ppm; H γ 2: 2.81 ppm) and the H δ protons of AcOHOrn4 (H δ 1: 3.80 ppm; H δ 2: 3.35 ppm) and AcOHOrn6 (H δ 1: 3.34 ppm; H δ 2: 3.73 ppm).

Structural Constraints. The relatively small size of azoverdin-Ga(III) (one chromophore and six amino acids) gave only few long-range distance constraints, which are critical for the structure determination. To overcome this limitation, a careful analysis of nuclear Overhauser interactions between the protons was undertaken (Figure 2A). The NOE between the protons H4 and H5 of the chromophore (used as a

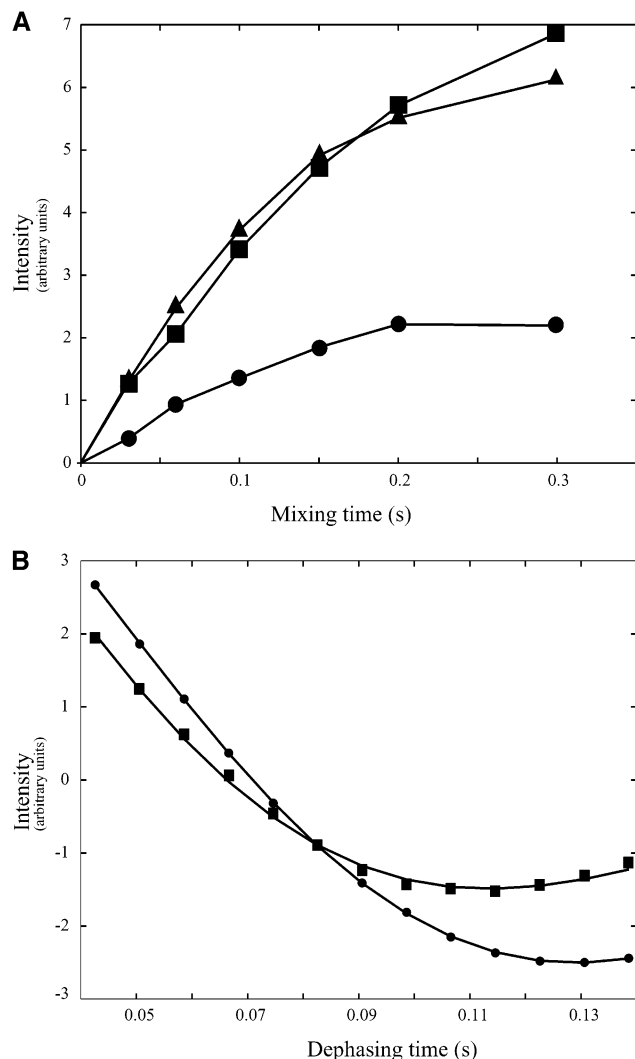


FIGURE 2: (A) NOE buildup curves from NOESY spectra with mixing times of 30, 60, 100, 150, 200, and 300 ms. Data shown are for Chr H4/Chr H5 (▲), Dab3 H α /AcOHOrn4 HN (■), and Dab3 H β 2/AcOHOrn4 HN (●). (B) Time evolution of ^1H - ^{15}N peak intensities for residues AcOHOrn4 (■) and AcOHOrn6 (●) measured on the ^1H - ^{15}N CT-HMQC-J spectra. The fit is indicated by a solid line.

reference for the distance calibration) was negative, and linearity of the buildup curve for mixing times lower than 100 ms indicated that the two-spin approximation could give an accurate estimate of the cross-relaxation rate. Taking an interproton distance of 2.42 Å between these protons, the buildup rate gave a rotational correlation time of 1.0 ns for azoverdin-Ga(III). All interproton distances were calibrated using this correlation time. Errors on the distances were set following a visual inspection of the buildup curves. For high-quality buildup curves, the upper and lower distance errors were set to 0.3 and 0.4 Å, respectively, whereas larger boundaries were used when significant deviations from linearity of the buildup curve were observed. All sequential HN-H α distances were determined with high precision, providing an accurate set of structural constraints on the peptide backbone and more specifically on the Φ dihedral angle. The folding of the peptide chain around the gallium ion was well constrained by 27 medium- and long-range distances (Table 1). $^3J_{\text{HN-H}\alpha}$ coupling constants were measured using constant-time ^1H - ^{15}N HMQC-J experiments to

Table 1: Experimental Restraints and Structural Statistics for the Family of 18 Calculated Structures of Azoverdin-Ga(III)

Restraints for Calculation	
total NOE restraints	82
intraresidue	36
sequential ($ i - j = 1$)	19
medium range ($1 < i - j < 4$)	15
long range ($ i - j > 4$)	12
hydrogen bond restraints	2
dihedral angle restraints	19
residual dipolar couplings	
$^1\text{D}_{\text{NH}}$	5
$^3\text{D}_{\text{HNH}\alpha}$	5
Structure Statistics ^a	
rmsd from idealized covalent geometry	
bonds (Å)	0.0097 ± 0.0002
bond angles (deg)	1.2071 ± 0.0079
improper torsions (deg)	2.0481 ± 0.0075
NOE restraints (Å)	0.0955 ± 0.0026
dihedral angle restraints (deg)	0.6499 ± 0.0024
residual dipolar couplings (hz)	0.3557 ± 0.0214
final energies (kcal.mol ⁻¹)	
E_{total}	192.9 ± 3.0
E_{bonds}	13.6 ± 0.7
E_{angles}	57.5 ± 0.7
E_{vdW}	9.9 ± 0.8
E_{NOE}	37.4 ± 2.0
E_{RDC}	21.6 ± 0.6
Coordinate Precision ^b (Å)	
rmsd of selected heavy atoms ^c	0.21

^a Structure statistics refers to the ensemble of 18 structures with the lowest energy from 30 calculated structures. ^b rmsd between the ensemble of 18 structures. ^c Selected heavy atoms are backbone, chromophore without succinate residue, 2,4-diaminobutyric acid, and both N $^{\delta}$ -acetyl-N $^{\delta}$ -hydroxyornithines and the gallium(III) ion.

Table 2: Coupling Constants and Residual Dipolar Couplings^a

residue	$^3J_{\text{HN-H}\alpha}$ 298 K	$^3J_{\text{HN-H}\alpha}$ 305 K	$^3J_{\text{HN-H}\alpha}$ 308 K	$^1J_{\text{NH}}$ 305 K	$^1J_{\text{NH}}$ 308 K
	no bicelles (Hz)	no bicelles (Hz)	bicelles (Hz)	no bicelles (Hz)	bicelles (Hz)
L-Chr	4.0	4.9	7.6	95.9	88.3
L-Hse1	5.5	5.4	8.5	93.7	99.5
D-Hse2	4.2	4.1	0.0	93.8	97.6
L-Dab3 (HN)	3.8	4.1	7.7	95.6	112.7
L-Dab3 (HN δ)	—	—	—	97.1	91.0
D-AcOHOrn4	7.5	8.2	9.6	92.3	107.1
D-Ser5	4.5	4.6	7.3	93.0	100.5
L-AcOHOrn6	7.5	6.5	5.2	91.5	95.1

^a The first column shows coupling constants measured on the original sample, from a series of ^{15}N - ^1H CT-HMQC spectra. For all other columns, measurements were made in 10 mM phosphate buffer, pH 6.5, 0.02% NaN₃, at 305 K without phospholipidic bicelles, and at 308 K with phospholipidic bicelles. $^3J_{\text{HN-H}\alpha}$ coupling constants were measured from a series of ^{15}N - ^1H CT-HMQC spectra and $^1J_{\text{NH}}$ from ^{15}N - ^1H HSQC spectra F2 cross-sections.

a precision of 0.1 Hz (Figure 2B and Table 2). When more than one Φ dihedral angle value corresponded to the measured $^3J_{\text{HN-H}\alpha}$ coupling constant (as for AcOHOrn4, Ser5 and AcOHOrn6), the appropriate values were determined during preliminary structure calculations. Additional structural constraints were obtained from hydrogen exchange analysis. Two-dimensional proton spectra recorded shortly after dissolution of azoverdin-Ga(III) in D₂O showed the persistence of two resonances which were assigned to the HN of AcOHOrn6 and the HN δ of Dab3. Hydrogen bonding partners were identified in early stages of the structure calculations.

Structure calculation strategy. The relative position of the three bidentate coordinating groups around the gallium ion defines the absolute configuration of the chiral center. Assuming an octahedral geometry of the coordination sphere, 16 configurations should be considered: eight coordination isomers with a Λ chirality and their eight mirror images with Δ chirality (10). In the examples of pyoverdins for which structures have been determined by NMR, a significant number of the possible geometries were excluded on the basis of steric hindrance. In azoverdin–Ga(III) however, two of the three coordinating groups are located at the end of long AcOHOrn side chains, allowing greater flexibility. Circular dichroism spectra have been used to determine the absolute configurations (Λ or Δ) of siderophores (14, 48), and the analysis of CD spectra of azoverdin–Fe(III) (15) suggested that the isopyoverdin adopted a predominantly Δ configuration. To avoid any bias in the structure determination of the gallium complex, we performed simulated annealing calculations using the 16 possible coordination isomers as starting points. For each of the 16 isomers, 30 initial structures were generated by constraining a perfect octahedron around the gallium ion using distance and dihedral angle constraints. These starting structures were subsequently subjected to a simulated annealing procedure where experimental interproton distance constraints as well as dihedral angle constraints were included as quadratic potential functions. A final energy minimization step was applied before selecting the final structures. The selection criteria were: no distance violation greater than 0.4 Å and no angle violation greater than 5°.

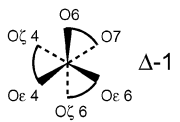
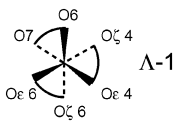
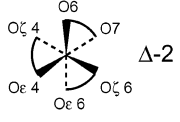
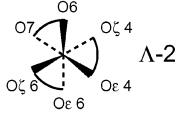
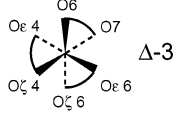
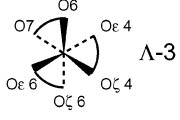
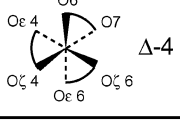
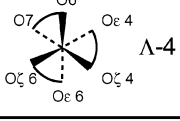
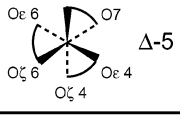
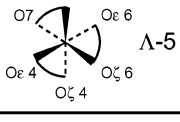
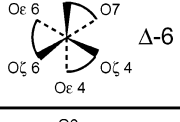
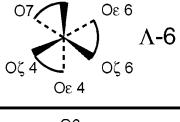
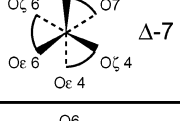
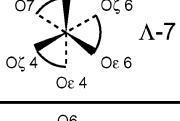
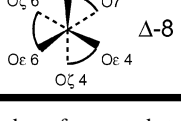
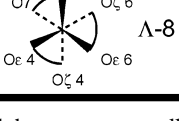
Of the 16 possible isomers, only isomer Δ -4 led to accepted structures, with a mean total energy of 76.6 kcal.mol⁻¹ (Table 3). All other geometries led to overall energies that were at least 1.6 times higher than the Δ -4 isomer and gave no accepted structures.

Structure Assessment Using Residual Dipolar Coupling Constants. The primary sequence of the azoverdin peptide chain contains AcOHOrn residues with both L and D configurations of their C α , the configurations being determined by gas chromatography of O-methyl, N-pentafluoropropionyl derivatives of amino acids after total hydrolysis (15). However, the ambiguity in the sequential location of the two AcOHOrn enantiomers remained since no experimental evidence was provided to discriminate between the sequences D-AcOHOrn4-D-Ser5-L-AcOHOrn6 and L-AcOHOrn4-D-Ser5-D-AcOHOrn6. In the calculation presented above, the former sequence published by Michalke et al. (16) was assumed. To confirm the chirality of the AcOHOrn residues in the sequence, additional structure calculations were performed with the alternate primary sequence. The same structure calculation protocol was used for both primary sequences (referred hereafter as DL or LD, depending on the order in the sequence of the D and L isomers of AcOHOrn), and the results of this second set of structure calculations are also presented in Table 3. Of the 16 coordination geometries, only Λ -7 fitted the experimental NOE and dihedral angle constraints and led to accepted structures. Despite a slightly higher overall energy level (84.4 kcal.mol⁻¹), this calculation showed that an azoverdin–Ga(III) model based on the L-AcOHOrn4-D-Ser5-D-AcOHOrn6 sequence topology could equally fit our experimental constraints.

The assessment of the chirality of the two AcOHOrn residues required additional structural information. We therefore decided to use orientational constraints from residual dipolar couplings (RDCs) in order to address this question. Residual dipolar couplings have proven to be very useful in defining the chirality of an asymmetric center in numerous cases (49). $^1J_{N-H}$ and $^3J_{HN-H\alpha}$ coupling constants were measured in a sample that was weakly oriented in a liquid crystalline medium (Table 2). Since some of the $^3J_{HN-H\alpha}$ coupling constants were slightly affected by temperature, the coupling constants measured in the absence of DMPC:DHPC at 305 K were used as isotropic reference values. The quadrupolar splitting of the deuterium signal from D₂O (10 Hz at 308 K) indicated that the transition to the nematic phase was successfully achieved, and the variations in the $^1J_{N-H}$ coupling constants values showed that partial orientation of azoverdin–Ga(III) molecule was obtained. The proton and nitrogen chemical shifts in the 1H - ^{15}N HSQC spectra recorded with and without DMPC:DHPC bicelles were similar, indicating that the structure of azoverdin–Ga(III) peptide was not affected by the phospholipids. The use of RDC data in structure calculations requires an estimate of the axial and rhombic components of the orientation tensor, usually obtained by analyzing the distribution of a large number of RDC values for vectors sampling many different orientations (31). This approach fails for azoverdin–Ga(III) due to the low number of N–H vectors. The rhombicity was therefore estimated from the inertia tensor eigenvalues calculated using the initial set of structures to be 0.52. The axial component was subsequently refined using a grid search procedure, and the best fit was obtained for a value of –16 Hz. The value of the axial component of the orientation tensor for RDC calculated from $^3J_{HN-H\alpha}$ coupling constants were deduced from this latter value.

For each HN–H α vector, a calibration factor was applied to take into account the interproton distance determined from analysis of the NOE buildup. Since no sign determination of the RDC contribution was possible for interproton vectors, only absolute values of the coupling constants measured in the anisotropic phase were considered. A second round of structure calculations was undertaken using the same protocol as above, but including the RDC constraints as an additional harmonic potential term in the energy function (50). The RDC values measured for Hse1 were not considered for this second calculation since specific dynamical averaging at the chromophore-peptide junction, as suggested by line broadening of some resonances (Figure 5B), may affect their accuracy. The results for the 32 topologies (16 LD isomers and 16 DL isomers) are shown in the Table 3. The consistency between distance, angular and orientational data is compatible with a unique topology: the Δ -4 geometry of the DL sequence. For this set of structures, very good agreement between experimental and calculated RDC values was observed (Figure 3), while distance constraints were also satisfied. No accepted structures were obtained for the LD topology. RDC constraints are less well satisfied, and violations of NOEs are observed. The chirality of the amino acids in the sequence was thus confirmed. The angle between the main axis of the inertia and orientational tensors was found to be 20.1° (Figure 4), suggesting that the rotational diffusion restriction was mainly due to steric interactions between the molecule and the bicelles.

Table 3: Summary of Azoverdin–Ga(III) Calculation Results^a

Δ ISOMERS	«D-L» SEQUENCE	«L-D» SEQUENCE	Λ ISOMERS	«D-L» SEQUENCE	«L-D» SEQUENCE
 Δ -1	$\begin{matrix} 0 \\ 1860 \pm 1839 \\ 0 \\ 588 \pm 191 \end{matrix}$	$\begin{matrix} 0 \\ 755 \pm 1113 \\ 0 \\ 526 \pm 55 \end{matrix}$	 Λ -1	$\begin{matrix} 0 \\ 681 \pm 1052 \\ 0 \\ 803 \pm 277 \end{matrix}$	$\begin{matrix} 0 \\ 1274 \pm 1514 \\ 0 \\ 1924 \pm 1376 \end{matrix}$
 Δ -2	$\begin{matrix} 0 \\ 238.0 \pm 16.7 \\ 0 \\ 358.1 \pm 37.9 \end{matrix}$	$\begin{matrix} 0 \\ 347.3 \pm 66.7 \\ 0 \\ 745 \pm 381 \end{matrix}$	 Λ -2	$\begin{matrix} 0 \\ 177.4 \pm 2.1 \\ 0 \\ 540 \pm 613 \end{matrix}$	$\begin{matrix} 0 \\ 332.7 \pm 29.4 \\ 0 \\ 1854 \pm 1129 \end{matrix}$
 Δ -3	$\begin{matrix} 0 \\ 910 \pm 1576 \\ 0 \\ 825 \pm 668 \end{matrix}$	$\begin{matrix} 0 \\ 134.9 \pm 13.1 \\ 0 \\ 389.6 \pm 70.4 \end{matrix}$	 Λ -3	$\begin{matrix} 0 \\ 671 \pm 769 \\ 0 \\ 2048 \pm 1927 \end{matrix}$	$\begin{matrix} 0 \\ 527 \pm 327 \\ 0 \\ 532 \pm 92 \end{matrix}$
 Δ -4	$\begin{matrix} 23 \\ 76.6 \pm 18.6 \\ 18 \\ 191.8 \pm 4.2 \end{matrix}$	$\begin{matrix} 0 \\ 484 \pm 307 \\ 0 \\ 900 \pm 794 \end{matrix}$	 Λ -4	$\begin{matrix} 0 \\ 310.5 \pm 8.1 \\ 0 \\ 487 \pm 23 \end{matrix}$	$\begin{matrix} 0 \\ 215.1 \pm 0.3 \\ 0 \\ 599 \pm 176 \end{matrix}$
 Δ -5	$\begin{matrix} 0 \\ 309.1 \pm 3.6 \\ 0 \\ 632 \pm 302 \end{matrix}$	$\begin{matrix} 0 \\ 126.6 \pm 1.3 \\ 0 \\ 429 \pm 0.1 \end{matrix}$	 Λ -5	$\begin{matrix} 0 \\ 125.8 \pm 0.6 \\ 0 \\ 272.9 \pm 3.9 \end{matrix}$	$\begin{matrix} 0 \\ 491 \pm 128 \\ 0 \\ 739 \pm 54 \end{matrix}$
 Δ -6	$\begin{matrix} 0 \\ 347.3 \pm 3.4 \\ 0 \\ 1728 \pm 713 \end{matrix}$	$\begin{matrix} 0 \\ 192.6 \pm 1.7 \\ 0 \\ 510 \pm 28.3 \end{matrix}$	 Λ -6	$\begin{matrix} 0 \\ 137.5 \pm 5.3 \\ 0 \\ 241.0 \pm 28.3 \end{matrix}$	$\begin{matrix} 0 \\ 325.2 \pm 332.4 \\ 0 \\ 608 \pm 423 \end{matrix}$
 Δ -7	$\begin{matrix} 0 \\ 218.7 \pm 2.8 \\ 0 \\ 479 \pm 129 \end{matrix}$	$\begin{matrix} 0 \\ 1024 \pm 1518 \\ 0 \\ 830 \pm 169 \end{matrix}$	 Λ -7	$\begin{matrix} 0 \\ 227.8 \pm 2.2 \\ 0 \\ 416.5 \pm 83.2 \end{matrix}$	$\begin{matrix} 18 \\ 84.4 \pm 14.1 \\ 0 \\ 386.6 \pm 0.1 \end{matrix}$
 Δ -8	$\begin{matrix} 0 \\ 237.1 \pm 2.6 \\ 0 \\ 416 \pm 98 \end{matrix}$	$\begin{matrix} 0 \\ 137.8 \pm 0.7 \\ 0 \\ 448 \pm 1 \end{matrix}$	 Λ -8	$\begin{matrix} 0 \\ 166.2 \pm 1.5 \\ 0 \\ 331.2 \pm 12.5 \end{matrix}$	$\begin{matrix} 0 \\ 228.8 \pm 2.4 \\ 0 \\ 439 \pm 105 \end{matrix}$

^a The number of accepted structures (out of 30 structures generated) and the average overall energy of the five best structures are shown for each coordination isomer, for calculations without (first and second line in italic) and with RDC data (last two lines). Results in bold indicate accepted isomers. The use of RDC allowed geometric ambiguities that remain with classical NMR constraints to be removed and confirmed the compatibility of NMR data with a unique topology, the Δ -4 geometry of the DL sequence.

A final check on the consistency between the three-dimensional model of azoverdin–Ga(III) and the experimental NOE data set was provided by a careful analysis of back-calculated NOESY spectra (Figure 5). Whereas no inconsistencies between experimental and back-calculated NOESY spectra (Figure 5A) could be found for the DL 4 Δ family, the theoretical spectrum calculated for the LD-7 Λ family (Figure 5C) displayed several NOEs that were not observed, in particular, that between the side chain of AcOHOrn6 and the H5 proton of the chromophore ring.

Tertiary Structure of Azoverdin–Ga(III) Complex. The three-dimensional structure of azoverdin–Ga(III) is shown in Figure 4, and the internal coordinates are provided in Table 4. The conformation of the peptide backbone and the side chains of residues involved in the coordination of the gallium ion are defined with a high precision (rmsd of 0.21 Å for

the backbone heavy atoms). The molecule is characterized by a U-shape, with the residues Hse1 and Ser5 located at the lower corners of the U. The peptide backbone, which is always located on the same side of the chromophore, forms a surprisingly large cradle and the two AcOHOrn side chains adopt an extended conformation in order to chelate the gallium ion. This particular conformation of the coordination center leaves a large open space, permitting access to the bound ion. The N-terminal corner of the U is stabilized by a hydrogen bond between the oxygen atom of the carbonyl group bound to C13 of the chromophore and the HN δ amide proton of Dab3, and its C-terminal corner is stabilized by a hydrogen bond between the carbonyl group of AcOHOrn4 and the amide proton of AcOHOrn6. Both these amide protons were seen to exchange slowly into D₂O. The three polar hydroxyl groups of Hse1, Hse2, and Ser5 are exposed

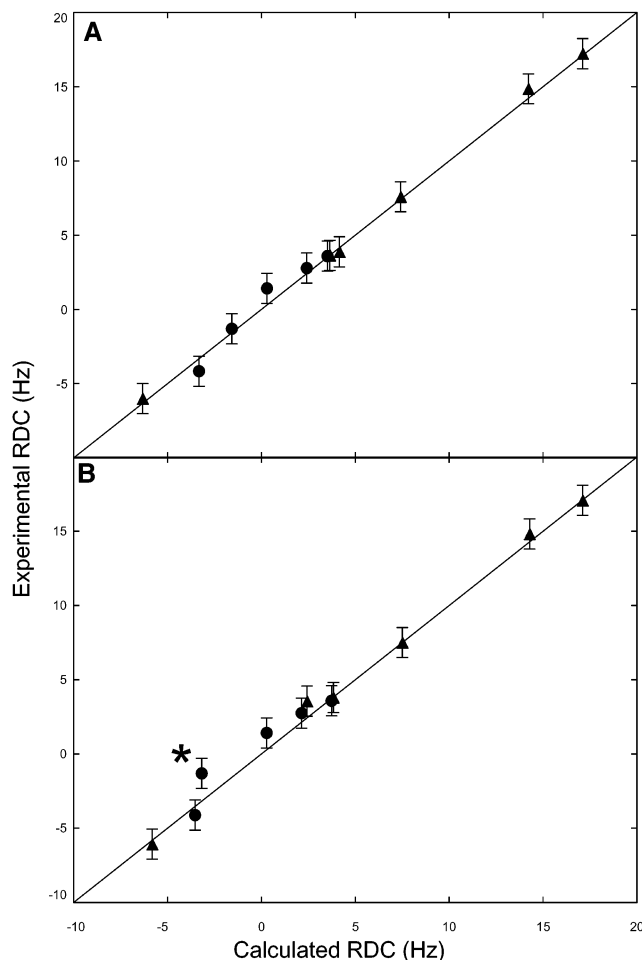


FIGURE 3: Measured and calculated dipolar couplings $^1D_{N-H}$ (\blacktriangle) and $^3D_{HN-H\alpha}$ (\bullet) for (A) the accepted structures of the DL- Δ 4 family and (B) the lowest-energy structures of the of the LD- Λ 7 family. The star indicates the D-AcOHOrn6 residue, of which $^3D_{HN-H\alpha}$ data display a significant discrepancy between experimental and calculated values.

to the solvent and probably contribute to a favorable solvation energy. The alignment of these three hydroxyl groups constitutes a striking feature of the azoverdin-Ga(III) structure and plays a probable role in receptor recognition.

DISCUSSION

The solution structure of azoverdin-Ga(III) presented in this paper represents the fourth three-dimensional structure of a peptidic siderophore at atomic resolution and the third structure of a gallium complex obtained by NMR (for review, see Folschweiller et al., 51). Two characteristic features of the azoverdin siderophore required the use of enhanced NMR methodology to obtain an accurate structure. First, in azoverdin, two of the chelating groups are located at the end of the long AcOHOrn side chains. The high degree of flexibility introduced by the four dihedral angles of these side chains rendered the definition of the chirality of the ion coordination center difficult. Second, the azoverdin is characterized by a different linkage site of the peptidic moiety to the chromophore, and ambiguities in the primary structure of this peptide were present at the beginning of this study. The production of ^{15}N -labeled azoverdin-Ga(III) allowed us to remove most of the ambiguities on the primary sequence of the peptide (29), with the exception of the

chirality of the C α atoms of the two AcOHOrn residues. This latter question was addressed by the use of residual dipolar coupling constants. The use of NMR data recorded on molecules dissolved in chiral liquid crystalline media to define the geometry of a chiral center was recently proposed and applied to small organic molecules (49). The results obtained on azoverdin-Ga(III) provide the first evidence that RDC data can be used to define the absolute configuration of amino acids present in a peptide of known structure. Although orientational constraints obtained from a single orientation of H_N-H_α and $N-H_N$ vectors were sufficient to define the geometry of the azoverdin-Ga(III) complex, it should be noted that more vectors could be used in the case of siderophores with more flexible peptide chains. Of particular interest are the vectors located in the vicinity of the gallium ion, such as $H_\delta-N_\epsilon$ or $N_\epsilon-C_\delta$ and $N_\epsilon-C_\zeta$, if a $^{15}N/^{13}C$ -labeled sample is available. The lifetime of azoverdin-Ga(III) dissolved in the liquid crystal medium did not allow us to record data for any additional vectors, but the use of other anisotropic media such as strained polyacrylamide gels (52) may allow us to overcome this problem.

The absolute configuration of the sphere of coordination can be established by CD spectroscopy. The selected Δ configuration for of azoverdin-Ga(III) which results from our set of NMR is in agreement with the interpretation of the CD spectral features of azoverdin-Fe(III) (15) which presents large similarities with the spectrum of ferric pseudobactin, showing a comparable intense positive Cotton effect at 400 nm. However, no positive Cotton effect at higher wavelength is observed in contrast to those shown by ferric pseudobactin B10 (10) and pyoverdin GMII-Fe(III) (14) in the same range, suggesting that like pyoverdin G4R-Fe(III) (48), azoverdin-Fe(III) complex is predominantly in a Δ absolute configuration.

Since azoverdin-Ga(III) is the first reported three-dimensional structure of an isopyoverdin, it is of particular interest to compare the structural consequences of this isomery. The four known structures of peptidic siderophores are shown in Figure 6 with the chromophore orientation identical in the four molecules. A first striking difference that emerges from this comparison is the path traced by the peptide backbone relative to the plane defined by the chromophore and the gallium ion (Figure 6). In all siderophores in which the peptide chain is bound to C11 of the chromophore, the backbone remains below the plane, surfacing to position the chelating ligands correctly to bind the metal ion. The opposite chirality at the C13 atom defines a reversed initial direction of the peptide chain in isopyoverdins. The peptide chain remains above the plane, dipping below only at the C-terminus to allow AcOHOrn6 to chelate the metal ion correctly. The position of the peptide chain relative to the gallium ion defines another specific feature of the azoverdin-Ga(III) structure. For pyoverdin structures, the peptide chain is wrapped around the gallium ion, whereas the peptide chain is located far from the ion in azoverdin-Ga(III), leaving a large open space for solvent accessibility. The two siderophores which contain a Dab residue (azoverdin and the *Pseudomonas putida* pyoverdin G4R) share the same Δ absolute configuration, whereas the coordination centers of pseudobactins B10 and GMII are characterized by Λ geometries. However, the observed geometry of the three

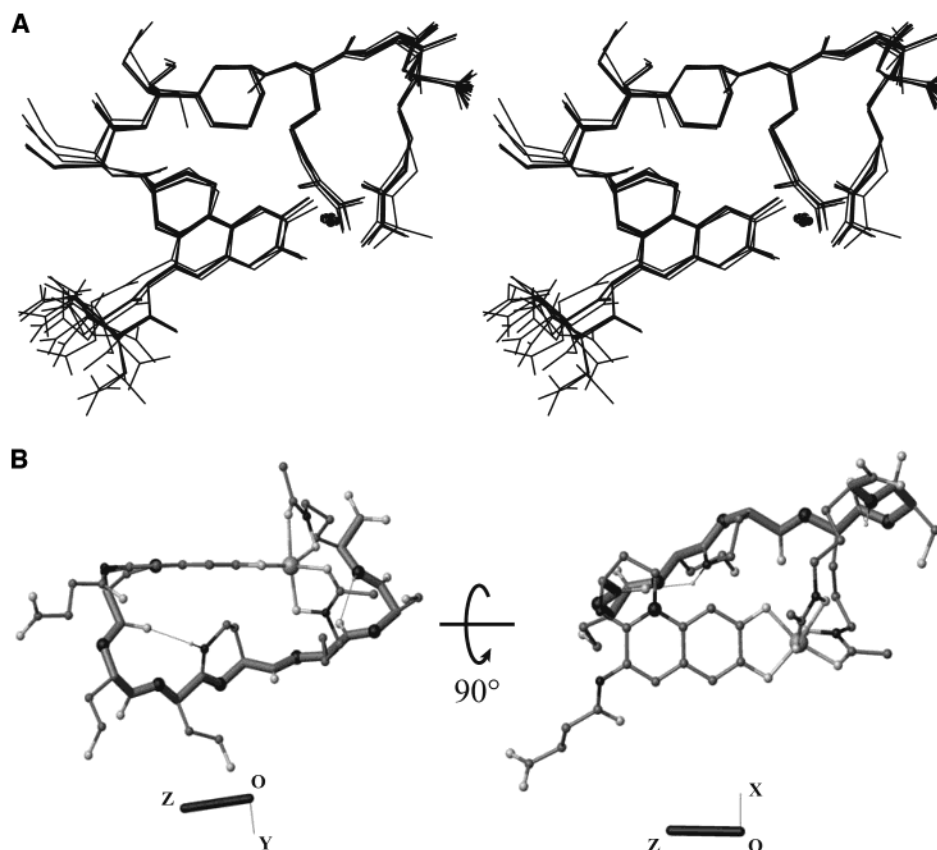


FIGURE 4: (A) Stereoview of the family of 18 accepted structures of azoverdin-Ga(III) (rmsd for backbone atoms = 0.21 Å). Ball-and-stick representation of the tertiary structure of azoverdin-Ga(III). (B) Only heavy atoms are represented, together with Dab3 HN δ and AcOHOrn6 HN protons, both involved in hydrogen bonds (dashed lines). The orientation tensor is shown with the OZ main axis drawn in bold.

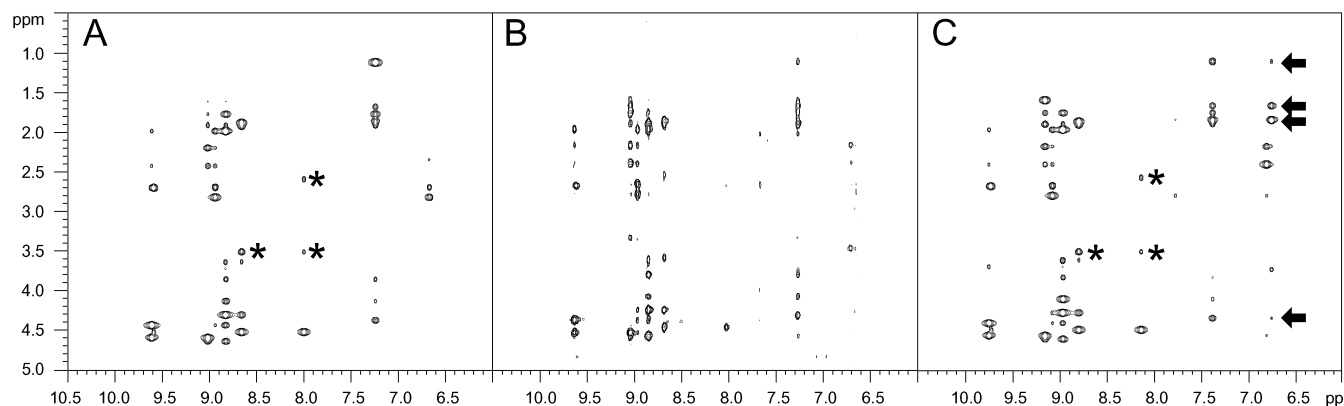


FIGURE 5: Comparison of experimental and back-calculated NOESY spectra for azoverdin-Ga(III). The HN-H α region of the experimental NOESY spectrum (mixing time of 200 ms) is shown in panel B, between the back-calculated spectra of DL-Δ4 (panel A) and LD-Δ7 (panel C) structures. Extra peaks in LD-Δ7 are indicated by arrows (←) and serve to confirm DL-Δ4 as the correct structure of azoverdin-Ga(III). Additional peaks in both panels A and C are indicated by asterisks and involve protons of the nonaromatic cycle of the chromophore.

bidendate groups around the metallic ion of the two former siderophores defines two different isomers, Δ-4 and Δ-6, respectively. A further comparison of the two molecules that contain a Dab residue sheds light on the structural role of this residue which results from the condensation of an amino acid with 2,4-diaminobutyric acid. In pyoverdine G4R-Ga(III), the sequence Dab4-Gly5 has an important structural role in reversing the direction of the peptide chain. In azoverdin-Ga(III), the Dab also plays a major conformational role in stabilizing the first turn of the peptide chain, as indicated by the protection of its H δ proton. The structural role of this particular residue is thus reinforced, and its direct

involvement in specific interactions with the receptor is doubtful.

One striking structural feature of azoverdin-Ga(III) is the alignment of the three hydroxyl groups of the Hse1, Hse2, and Ser5, which may be a specific feature recognized by the azoverdin receptor. A review of pyoverdine sequences (9) shows that hydroxylated residues are present in high frequency. While certain of these side chains may be involved in metal ion chelation, others may play a role in defining siderophore specificity at the receptor. Despite the availability of three crystallographic structures of siderophore outer membrane receptors FhuA, FepA, and FecA (53–56)

Table 4: Statistics on Dihedral Angles^a

residue	Φ (deg)	ψ (deg)	χ_1 (deg)	χ_2 (deg)	χ_3 (deg)	χ_4 (deg)
Chr	56.2 ± 0.1	82.6 ± 0.2	52.9 ± 0.1	-16.7 ± 0.2	—	—
Hse1	-55.6 ± 0.1	80.8 ± 0.1	-167.8 ± 0.2	-132.8 ± 0.2	—	—
Hse2	158.0 ± 0.1	-173.8 ± 0.5	170.7 ± 52.3	138.9 ± 49	—	—
Dab3	91.1 ± 0.0	157.5 ± 0.0	59.7 ± 0.2	-56.0 ± 0.3	26.2 ± 0.5	2.8 ± 0.5
AcOHOrn4	-170.0 ± 0.1	177.1 ± 0.1	106.6 ± 0.4	139.9 ± 0.1	49.1 ± 0.1	-160.5 ± 0.1
Ser5	31.8 ± 0.3	40.3 ± 0.6	-34.1 ± 44.3	—	—	—
AcOHOrn6	-61.4 ± 0.2	—	70.4 ± 0.2	168.3 ± 0.02	119.9 ± 0.1	163.8 ± 0.2

^a For the chromophore, dihedral angles χ_1 and χ_2 are defined by N_{14} , C_{13} , C_{12} , C_{11} and by C_{13} , C_{12} , C_{11} , N_1 , respectively. For the Dab3 residue, dihedral angles χ_3 and χ_4 are defined by C_β , C_γ , N_δ , C' and by C_γ , N_δ , C' , NH , respectively.

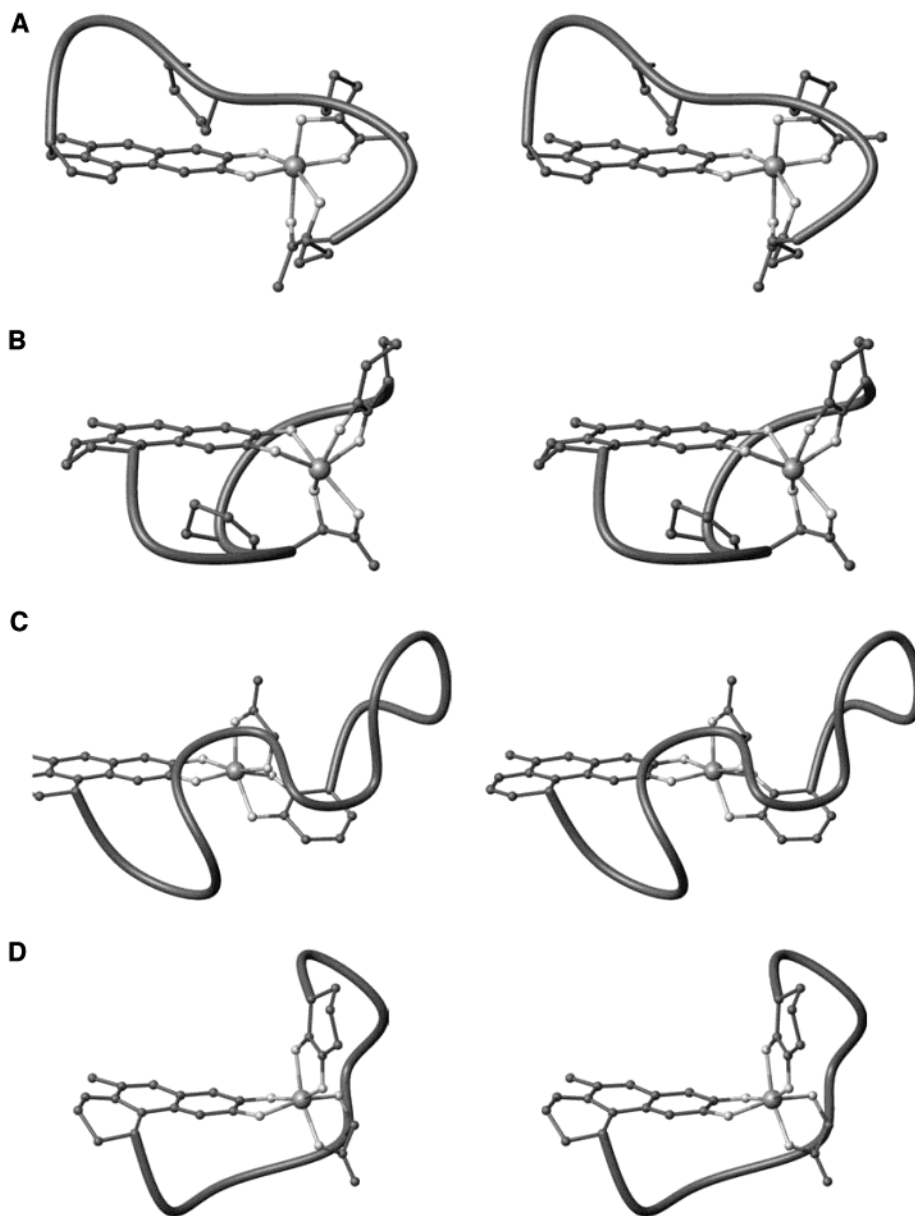


FIGURE 6: Comparison of the structure of azoverdin-Ga(III) with the three known pyoverdins: stereoviews of (A) azoverdin-Ga(III), (B) pyoverdins G4R-Ga(III), (C) pyoverdins GMII-Ga(III) and (D) ferric pseudobactin. The four structures are presented such that the chromophore is in the same orientation.

and four pyoverdins and isopyoverdins structures, the structural basis of the specificity of pyoverdins-receptor recognition remains an open question.

The structural features of azoverdin-Ga(III) emphasize the structural diversity of this class of siderophores. This is a direct result of the known diversity of the peptide sequences of pyoverdins. The structural work performed on azoverdin-

Ga(III) exploited several NMR techniques which were developed for protein applications, such as the triple resonance HNCA experiment and the use of orientational constraints. We have shown that residual dipolar couplings may be obtained from pyoverdins molecules dissolved in bicelle media. The use of this kind of structural information may be extensively developed in the future to speed up the

structure determination process of these small peptides which is currently rather time-consuming. By analyzing the structures of many siderophores, we aim to define common features that form a general basis for bacterial iron transport and understand the specificity of particular siderophores for their own receptors.

ACKNOWLEDGMENT

The authors wish to thank C. Ling for his experimental assistance and G. Kelly (NIMR, London) for his help with the use of RDC constraints in X-PLOR.

REFERENCES

- Jensen, H. L. (1955) *Acta Agric. Scand.* 5, 280–294.
- Page, W. J., and Collinson, S. K. (1987) *Can. J. Microbiol.* 33, 830–833.
- Kim, J., and Rees, D. C. (1994) *Biochemistry* 33, 389–397.
- Chan, Y.-K. (1991) *Can. J. Microbiol.* 37, 715–718.
- Lankford, C. E. (1973) *CRC Crit. Rev. Microbiol.* 2, 273–331.
- Neilands, J. B. (1982) *Annu. Rev. Microbiol.* 36, 285–309.
- Collinson, S. K., Abdallah, M. A., and Page, J. W. (1990) *J. Gen. Microbiol.* 136, 2297–2305.
- Collinson, S. K., and Page, J. W. (1989) *J. Gen. Microbiol.* 135, 1229–1231.
- Pattus, F., and Abdallah, M. A. (2000) *J. Chin. Chem. Soc.* 47, 1–20.
- Teintze, M., Hossain, M. B., Barnes, C. L., Leong, J., and van der Helm, D. (1981) *Biochemistry* 20, 6446–6457.
- Persmark, M., Frejd, T., and Mattiasson, B. (1990) *Biochemistry* 29, 7348–7356.
- Demange, P., Bateman, A., MacLeod, J. K., Dell, A., and Abdallah, M. A. (1990) *Tetrahedron Lett.* 31, 7611–7614.
- Demange, P., Bateman, A., Mertz, C., Dell, A., Piémont, Y., and Abdallah, M. A. (1990) *Biochemistry* 29, 11041–11051.
- Mohn, G., Koehl, P., Budzikiewicz, H., and Lefèvre, J.-F. (1994) *Biochemistry* 33, 2843–2851.
- Bernardini, J. J., Linget-Morice, C., Hoh, F., Collinson, S. K., Kyslik, P., Page, W. J., Dell, A., and Abdallah, M. A. (1996) *BioMetals* 9, 107–120.
- Michalke, R., Taraz, K., and Budzikiewicz, H. (1996) *Z. Naturforsch.* 51c, 772–780.
- Salah El Din, A. M., Kyslik, P., Stephan, D., and Abdallah, M. A. (1997) *Tetrahedron* 53, 12539–12552.
- Poppe, K., Taraz, K., and Budzikiewicz, H. (1987) *Tetrahedron* 43, 2261–2272.
- Briskot, G., Taraz, K., and Budzikiewicz, H. (1989) *Liebigs Ann. Chem.* 375–384.
- Demange, P., Wendenbaum, S., Linget, C., Mertz, C., Cung, M. T., Dell, A., and Abdallah, M. A. (1990) *Biol. Metals* 3, 155–170.
- Hohlneicher, U., Hartmann, R., Taraz, K., and Budzikiewicz, H. (1992) *Z. Naturforsch.* 47b, 1633–1638.
- Geisen, K., Taraz, K., and Budzikiewicz, H. (1992) *Monats. Chem.* 123, 151–178.
- Linget, C., Azadi, P., MacLeod, J. K., Dell, A., and Abdallah, M. A. (1992) *Tetrahedron Lett.* 33, 1737–1740.
- Linget, C., Stylianou, D. G., Dell, A., Wolff, R. E., Piémont, Y., and Abdallah, M. A. (1992) *Tetrahedron Lett.* 33, 3851–3854.
- Hohlneicher, U., Hartmann, R., Taraz, K., and Budzikiewicz, H. (1995) *Z. Naturforsch.* 50c, 337–344.
- Wong-Lun-Sang, S., Bernardini, J. J., Hennard, C., Kyslik, P., Dell, A., and Abdallah, M. A. (1996) *Tetrahedron Lett.* 37, 3329–3332.
- Yang, C. C., and Leong, J. (1984) *Biochemistry* 23, 3534–3540.
- Linget, C., Collinson, S. K., Azadi, P., Dell, A., Page, W. J., and Abdallah, M. A. (1992) *Tetrahedron Lett.* 33, 1889–1892.
- Wasielewski, E., Abdallah, M. A., Kyslik, P., and Kieffer, B. (2001) *C. R. Acad. Sci. Paris* 4, 765–770.
- Tjandra, N., and Bax, A. (1997) *Science* 278, 1111–1114.
- Clore, G. M., Gronenborn, A. M., and Bax, A. (1997) *J. Magn. Reson.* 133, 216–221.
- Page, W. J., and Sadoff, H. L. (1976) *J. Bacteriol.* 125, 1080–1087.
- Dobisova, M., Abdallah, M. A., and Kyslik, P. (1994) *Appl. Environ. Microbiol.* 60, 4605–4607.
- Rance, M., Sørensen, O. W., Bodenhausen, G., Wagner, G., Ernst, R. R., and Wüthrich, K. (1983) *Biochem. Biophys. Res. Commun.* 117, 479–485.
- Bax, A., and Davis, D. G. (1985) *J. Magn. Reson.* 61, 306–320.
- Jeener, J., Meier, B. H., Bachmann, P., and Ernst, R. R. (1979) *J. Chem. Phys.* 71, 4546–4553.
- Desvaux, H., Berthault, P., Birlirakis, N., and Goldman, M. (1993) *C. R. Acad. Sci. Paris* 317, 19–25.
- Shaka, A. J., Barker, P. B., and Freeman, R. (1985) *J. Magn. Reson.* 64, 547–554.
- States, D. J., Haberkorn, R. A., and Ruben, D. J. (1982) *J. Magn. Reson.* 48, 286–292.
- Piotto, M., Saudek, V., and Sklenář, V. (1992) *J. Biomol. NMR* 2, 661–665.
- Kuboniwa, H., Grzesiek, S., Delaglio, F., and Bax, A. (1994) *J. Biomol. NMR* 4, 871–878.
- Marion, D., Ikura, M., Tschudin, R., and Bax, A. (1989) *J. Magn. Reson.* 85, 393–399.
- Wider, G., Neri, D., Otting, G., and Wüthrich, K. (1989) *J. Magn. Reson.* 85, 426–431.
- Kay, L. E., Ikura, M., Tschudin, R., and Bax, A. (1990) *J. Magn. Reson.* 89, 496–514.
- Brünger, A. T. (1992) *X-PLOR software Manual*, version 3.1, Yale University Press, New Haven, CT.
- Clore, G. M., Gronenborn, A. M., and Tjandra, N. (1998) *J. Magn. Reson.* 131, 159–162.
- Koradi, R., Billeter, M., and Wüthrich, K. (1996) *J. Mol. Graph.* 14, 51–55.
- Atkinson, R. A., Salah El Din, A. L., Kieffer, B., Lefèvre, J.-F., and Abdallah, M. A. (1998) *Biochemistry* 37, 15965–15973.
- Aroulanda, C., Merlet, D., Courtieu, J., and Lesot, P. (2001) *J. Am. Chem. Soc.* 123, 12059–12066.
- Tjandra, N., Omichinski, J. G., Gronenborn, A. M., Clore, G. M., and Bax, A. (1997) *Nat. Struct. Biol.* 4, 732–738.
- Folschweiller, N., Schalk, I. J., Celia, H., Kieffer, B., Abdallah, M. A., and Pattus, F. (2000) *Mol. Membr. Biol.* 17, 123–133.
- Sass, H.-J., Musco, G., Stahl, S. J., Wingfield, P. T., and Grzesiek, S. (2000) *J. Biomol. NMR* 18, 303–309.
- Ferguson, A. D., Hofmann, E., Coulton, J. W., Diederichs, K., and Welte, W. (1998) *Science* 282, 2215–2220.
- Locher, K. P., Rees, B., Koebnik, R., Mitschler, A., Moulinier, L., Rosenbusch, J. P., and Moras, D. (1998) *Cell* 95, 771–778.
- Buchanan, S. K., Smith, B. S., Venkatramani, L., Xia, D., Esser, L., Palnitkar, M., Chakraborty, R., van der Helm, D., and Deisenhofer, J. (1999) *Nat. Struct. Biol.* 6, 56–63.
- Ferguson, A. D., Chakraborty, R., Smith, B. S., Esser, L., van der Helm, D., and Deisenhofer, J. (2002) *Science* 295, 1715–1719.

BI025990A